Large slippage and depletion layer at the polyelectrolyte/solid interface

Chloé Barraud, Benjamin Cross, Cyril Picard, Fréderic Restagno, Lilianne Léger, Elisabeth Charlaix

Large slippage and depletion layer at the polyelectrolyte/solid interface

Chloé Barraud,[a] Benjamin Cross, [a] Cyril Picard,[a] Fréderic Restagno,[b] Lilianne Léger [b] and Elisabeth Charlaix *[a]

The slippage of polymer solutions on solid surfaces is often attributed to a depletion layer whose origin, thickness, and interaction with the flow are poorly understood. Using a Dynamic Surface Force Apparatus we report a structural and nanorheological study of the interface between hydrolyzed polyacrylamide solutions and platinum surfaces. Polyelectrolyte chains adsorb on the surfaces in a thin charged layer, acting as a nonattractive wall for the bulk solution. We investigate the flow of the viscoelastic solution on the adsorbed layer from the nanometer to 10 micrometers, bridging microscopic to macroscopic properties. At distances larger than 200 nanometers, the flow is well described by an apparent slip boundary condition. At smaller distance the apparent slip is found to decrease with the gap. In contrast to the apparent slip model, we show that a 2-fluids model taking into account the finite thickness of depletion layers at the non-attractive wall describes accurately the dynamic forces over 4 spatial decades of confinement. Depletion layers are found to be an equilibrium property of the interface, independent on the flow and on the confinement. Their thickness is phenomenologically described by $\xi + 2l_D$ with ξ the correlation length of the semi-dilute solutions and l_D the Debye length. We interpret this result in terms of screened repulsion between the charged adsorbed layer and the bulk polyions.

1 Introduction

Complex fluids are known to have a complex rheological behaviour, but their mechanical properties at interfaces are at least as complex as their bulk counterpart.[1–3] Interfaces are able to modify the structure and composition of complex fluids with respect to their bulk organisation owing to various sterical, electrostatic, and long-range interactions with the neighbouring phase,[4] impacting their vicinal rheology with major consequences for their flow properties even at the macroscopic scale. A generic question in the study of complex fluids is therefore to relate their structure and organisation at interfaces to their interfacial mechanical properties. In the last twenty years numerous studies have focused on the mechanical properties of complex fluids at the liquid/vapour interface.[5] However the solid interface, although of great practical importance for the manipulation of complex fluids in small size devices or in porous media, is much less understood. Buried between two condensed phases, solid/liquid interfaces are not directly accessible for structural characterisation. In this respect neutron reflectivity has been shown to be a unique tool for structural studies of soft matter/solid interfaces.[6] On the mechanical side, characterising liquid/solid interfaces requires to measure the interfacial motion under controlled stress, *i.e.*, measuring slip lengths.[7] However applying controlled stresses to the interface while disentangling the interfacial response from the bulk is notoriously difficult, and is not currently done while characterising the interfacial structure. Therefore mechanical studies of liquid/solid interfaces have mainly concentrated on simple liquids[7] and on polymer melts in the Newtonian regime.[8–12]

In this paper we show that concomittent equilibrium and dynamic surface force measurements, performed here with the dynamic Surface Force Apparatus (dSFA) but which can also be done with the Colloidal Probe AFM, allow to characterise surface interactions, structure and rheology, shedding a new light on the interfacial properties of complex fluids.

We study more specifically the case of polyelectroyte solutions which are of central interest in many industrial applications such as oil recovery, food processing, ski, cosmetics, lubricant formulations, but are also of interest in biophysics and biotechnologies in relation to DNA solutions.[13–16] As widely used rheo-thickening agents, the flow properties of polyelectrolyte solutions have been early investigated in confined geometries or mesopores, and it was shown that a depletion layer at the liquid/solid interface confers to the solution an ''effective'' viscosity lower than the bulk viscosity.[17,18] This is due to an apparent slip of the flow at the solid surface[1,7] which has been

[a] *Univ. Grenoble Alpes, CNRS, LIPhy, 38000 Grenoble, France. E-mail: elisabeth.charlaix@univ-grenoble-alpes.fr*
[b] *Laboratoire de Physique des Solides, CNRS, Univ. Paris-Sud, Université Paris-Saclay, 91405 Orsay Cedex, France*

investigated with various materials and configurations, such as sintered glass disks, porous membranes, single glass capillaries, electro-osmotic flows.[15,19–23] Neutron reflectivity was also used to characterise depletion layers:[24] their structural thicknesses were found comparable to the relevant structural length of the bulk polymer solution, *i.e.*, the gyration radius of the free polymer coil in dilute solutions, or the correlation length ξ in semi-dilute solutions.[25] However thickness values e of depletion layers obtained from hydrodynamic measurements, using the classical expression of the apparent slip length:[26]

$$b = e\left(\frac{\eta}{\eta_s} - 1\right) \tag{1}$$

where η and η_s are respectively the solution and solvent viscosity, have been in debate since the 1980s.[1,27] In some cases hydrodynamic depletion layers were found close to the structural scale of the bulk polymer solution.[17,28,29] But in other cases, they were found much larger than any possible structural size characterising the solution or its interaction with the solid wall.[14,15,30] Such thick depletion layers were attributed to the migration of chains under flow and hydrodynamic stress. These migration effects have lately received larger attention thanks to the development of nanofluidic devices where people have studied the migration of DNA solutions[13–16] and developed numerical models.[31–33]

In the present paper we have studied partially hydrolysed polyacrylamide (HPAM) viscoelastic solutions, which were previously shown to develop anomalously thick depletion layers.[15,30] Using equilibrium and dynamic surface force measurements, we highlight two main results. A first result is that the polyelectrolyte solution can develop a depletion layer upon its own adsorbed layer. The reason is that the adsorption of chains overcharges the surface with the same sign as the macro-ions, repelling them from the interface. The second result is that the flow of the solution on the solid surface is well described from the nanometer to several micrometers by a single, fully equilibrium depletion layer, whose thickness is found experimentally equal to $2l_D + \xi$, where ξ is the correlation length of the solution and l_D the Debye's length characterising its interaction with the wall. In order to establish this result, we show that the viscous dissipation of complex fluids in the presence of a depletion layer must be modelled carefully. First at large scale, the concept of slip length is not appropriate and the original Navier's partial slip formulation should be used, involving an interfacial friction coefficient. Second at smaller scale the finite thickness of the depletion layers needs to be taken into account as soon as the gap width becomes of the same order of magnitude as the equivalent slip length expressed by eqn (1), as the partial slip model utterly underestimates the actual viscous dissipation at smaller scale. Hydrodynamic measurements of depletion layers issued from slip lengths and showing anomalously large thicknesses could suffer from this bias.

2 Materials and methods

2.1 Polyelectrolyte solutions and surfaces

We study aqueous solutions of partially hydrolysed polyacrylamide (HPAM). HPAM is a water-soluble polyelectrolyte well-known for its viscosifying properties at small concentration, and widely used in the field of enhanced oil recovery and water purification.[34,35]

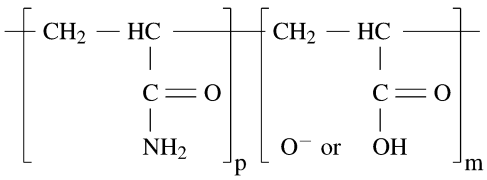

Fig. 1 Partially hydrolysed polyacrylamide.

HPAM forms a linear chain of acrylamide monomers, a fraction of which presents a carboxylate group (Fig. 1). The molar mass of the monomer is $M_A = 71.25$ g mol^{-1}, and its size is $a \approx 4$ Å. We use HPAM of molecular weight 2×10^7 g mol^{-1} (from SNF Flopaam 3630S) prepared in deionised water solution, in the concentration range around 1 g l^{-1}. In these conditions, which were otherwise well characterised by other groups,[30] the carboxyl groups are fully ionised, and the fraction of charged monomers on the chains is $f = m/(m + p) \approx 0.25$.

In the range of concentration studied, the solutions are expected to be in the semi-dilute entangled regime. The entanglement criterion for a semi-dilute solution is $C \geq C_e = n^4 C^*$, where $5 \leq n \leq 10$ is the average number of chains with which a given chain is overlapping, and C^* (in g l^{-1}) is the overlap concentration.[36]

$$C^* \approx (afN)^{-2} {l_B}^{-1} M_A / \mathcal{N}_A 10^3 \tag{2}$$

Here $N = 280\,700$ is the number of monomers in a chain, $\mathcal{N}_A$ is the Avogadro number, and $l_B = e^2/4\pi\varepsilon_w\varepsilon_o k_B T$ is the Bjerrum length.[36] At the experimental temperature $T = 28$ °C, with the relative dielectric constant of water $\varepsilon_w = 77.22$,[37] the Bjerrum length is $l_B = 7.2$ Å and $C^* = 0.16$ µg l^{-1} for the 20×10^6 g mol^{-1} HPAM. The criterion for entangled semi-dilute solutions is fully met with a calculated number of contacts $n = 50$. The correlation length in these solutions is:[36]

$$\xi \approx (af)^{-1/3} {l_B}^{-1/6} (C \mathcal{N}_A 10^3 / M_A)^{-1/2} \tag{3}$$

giving $\xi = 23 C^{-1/2}$ in nanometers, with C in g l^{-1}.

HPAM solutions are confined between a sphere and a plane. The surfaces are made of highly smooth floated borosilicate glass with a typical roughness of 2 Å over a 100 µm^2 area, measured by atomic force microscopy. They are then coated by a 6 nm thickness layer of chromium, and then by a 30 nm thickness layer of platinum. These metallic layers are deposited by magnetron sputtering. The typical roughness of the coating is less than 5 Å rms over a 100 µm^2 area.

2.2 Dynamic surface force apparatus (DSFA)

The experimental setup is a new Dynamic Surface Force Apparatus (DSFA) that can be used as a nanorheometer.[38] This DSFA measures separately the relative displacement h between a plane and a sphere (here of radius $R = 3.3$ mm), and the interaction force between them. The distance between the sphere and the plane can be tuned over a range of 15 µm. In addition the sphere can be oscillated with a small amplitude in the direction normal

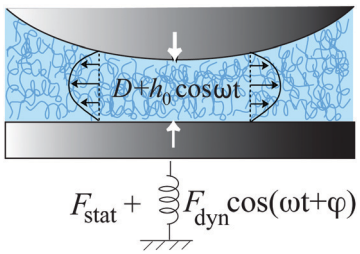

Fig. 2 Schematic of the dynamic surface force apparatus.

to the plane at a frequency $\omega/2\pi$ ranging from 30 Hz to 250 Hz. The relative distance between the sphere and the plane, measured with an interferometer, is resolved in its quasi-static component D, and the amplitude h_0 of the harmonic part. Similarly the independent measurement of the interaction force gives its quasi-static component F_{stat} (zero-frequency) and its dynamic component in amplitude and phase F_{dyn} and φ at angular frequency ω (see Fig. 2). In the dynamic regime, the displacement sensibility is 1 pm, the force sensibility is 10 nN, and the bandwidth is 1 Hz.

The zero-frequency component $F_{stat}(D)$ of the interaction force is related to the free energy $W(D)$ of the polymer solution confined between two parallel plates, by the Derjaguin approximation:[39]

$$\frac{F_{stat}(D)}{R} = 2\pi W(D) \tag{4}$$

The ω-harmonic force component $F_{dyn}\cos(\omega t + \varphi)$ is proportional to h_0 in the limit of linear response ($h_0 \ll D$) and defines a mechanical impedance $\tilde{Z}(D,\omega) = F_{dyn}\exp(i\varphi)/h_0 = Z_R + iZ_I$.

In the following we use the sphere complex mobility:

$$\tilde{\mu}(D,\omega) = \frac{\dot{D}}{F_{dyn}\exp(i\varphi)} = \frac{i\omega h_0}{F_{dyn}\exp(i\varphi)} \tag{5}$$

The sphere mobility allows one to probe the bulk linear rheology of the liquid as well as its boundary condition at the solid interface. For a visco-elastic liquid of complex viscosity $\tilde{\eta} = \tilde{G}/i\omega$ undergoing a no-slip boundary condition, the expected sphere mobility is $\tilde{\mu}(D,\omega)R^2 = D/(6\pi\tilde{\eta})$. Thus the bulk moduli of the visco-elasticity can be obtained from the slope of the linear growth of the reduced mobility $\mu(D,\omega)R^2$ at large gap D. In the case of a Navier's partial slip boundary condition:

$$\lambda \tilde{V}_{slip} = \tilde{\eta}\frac{\partial \tilde{V}_x}{\partial z} \tag{6}$$

characterised by the Navier interfacial friction coefficient λ, the reduced mobility is:[40]

$$R^2\tilde{\mu}(D) = \frac{D}{6\pi\tilde{\eta}}\frac{1}{f^*\left(\tilde{\eta}/\tilde{\lambda}D\right)}$$
$$f^*(\tilde{y}) = \frac{1}{3\tilde{y}}\left(\left(1+\frac{1}{6\tilde{y}}\right)\ln(1+6\tilde{y}) - 1\right) \tag{7}$$

reducing at large distance $D \gg |\tilde{\eta}/\lambda|$ to the affine variation

$$R^2\tilde{\mu}(D) \simeq \frac{D}{6\pi\tilde{\eta}} + \frac{1}{3\pi\tilde{\lambda}} \tag{8}$$

This expression also holds for a visco-elastic interfacial friction $1/\tilde{\lambda} = 1/\lambda_R + i\omega/k$ accounting for a dissipative interfacial friction λ_R and a finite interfacial compliance of stiffness k.

3 Equilibrium structure of the solution/solid interface

After a first cycle of approach, contact and withdrawal of the surfaces which is singular, the subsequent cycles are highly reproducible. This first cycle irreversibility has already been observed in SFA studies of various polyelectrolytes confined between oppositely charged or neutral surfaces.[41] In the following we present and discuss only the reproducible cycles after the first one.

Fig. 3 shows the typical interaction force, normalized by the sphere radius R, F_{stat}/R measured in HPAM solutions.

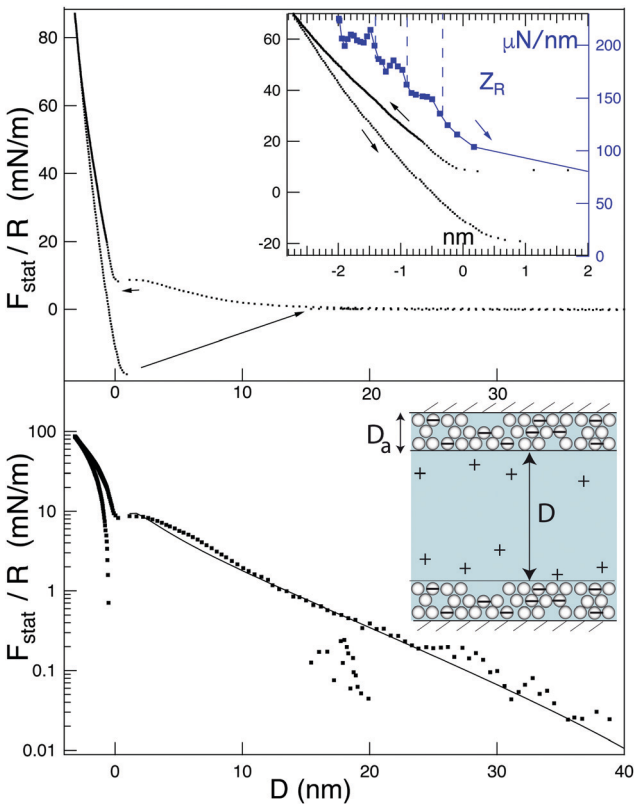

Fig. 3 Top: Reduced equilibrium force F_{stat}/R measured in a HPAM solution of 0.8 g l^{-1} concentration, as a function of the distance between the surfaces. The distance origin is set to the reception of the jump-to-contact of the advancing force (small arrow). Inset: Enlargement close to contact. The right axis of the inset plots in blue squares the dynamic stiffness Z_R in μN nm^{-1} measured at 220 Hz during the receding motion of the surfaces. Down: Reduced equilibrium force F_{stat}/R plotted in log-linear scale. The continuous line is the DLVO force at constant surface charge of 31 mC m^{-2} with a Debye's length l_D = 5.8 nm and a Hamaker constant 3 × 10^{-20} J.

Upon approaching the surfaces a repulsion interaction starts at a distance of around 20 nm from contact, followed by a jump-to-contact. We define arbitrarily the origin of the sphere-plane distance at the reception of this jump, which is a well-defined experimental point. However this origin is not a platinum-platinum contact: the stiffness Z_R beyond the origin increases by discrete steps, showing that the contact occurs on adsorbed polyelectrolyte chains. The size of the steps can be estimated to 5.2 Å, which is close but slightly larger than the monomer size $a \approx 4$ Å. The adsorbed layer is thus quite a flat layer. This is expected and observed for the adsorption of polyelectrolytes from a low ionic strength solution.[36,41] More specifically, the structure of adsorption layers of polyelectrolytes on charged surface of the opposite sign has been theoretically investigated, and shown to be comparable to a two-dimensional strongly correlated Wigner liquid.[42,43] In our case the surfaces are metallic, and the main attractive force acting on the polyelectrolyte chains is the image charge of opposite sign. The interaction with a metallic surface has been shown to be equivalent to the interaction with a charged surface of equivalent charge per area[36]

$$\frac{\sigma_{\text{eff}}}{e} = \left(\frac{f}{u}\right)^{1/3} \frac{1}{2l_D a^{2/3}} \quad u = \frac{l_B}{a} \tag{9}$$

with e the electronic charge and l_D the Debye's length. The thickness D_a of the adsorbed layer in this case is:[36]

$$D_a = \frac{a^{2/3}}{(l_B f \sigma/e)^{1/3}} = a\left(\frac{2l_D}{a^{1/3} l_B^{2/3} f^{4/3}}\right)^{1/3} \tag{10}$$

With the value of the Debye length $l_D = 5.8$ nm at $C = 0.8$ g l^{-1} (see below) one get $D_a = 4.99$, $a \approx 2$ nm. This corresponds indeed to thin adsorbed layers, in coherence with our observations.

On separating the surfaces a significant adhesion is measured, corresponding to a F_{stat}/R ratio of 19 mN m^{-1}, and to an interfacial tension $\gamma_{SL} = F_{stat}/4\pi R = 1.6$ mN m^{-1}. It is usually considered that the adhesion force between polyelectrolyte adsorbed layers increases strongly with the charge density of the polyelectrolyte, and F_{stat}/R ratios as high as 100–200 mN m^{-1} were observed for a charge fraction $f = 1$ on mica.[41] The magnitude found here for HPAM of charge fraction $f = 0.25$ is in coherence with this tendancy.

As shown on Fig. 3b the repulsion interaction on approaching the surfaces is comparable in amplitude to a DLVO interaction. In Fig. 3b ($C = 0.8$ g l^{-1}) the Debye's length is 5.8 nm and the surface charge is 31 mC m^{-2}. Double Layer force were previously measured in polyelectrolyte solutions with the SFA.[44] We have used here a DLVO calculation for a monovalent electrolyte, although there is no added salt in the solution, and the polyelectrolyte itself is not exactly a monovalent electrolyte. We justify this choice by the fact that the electrical double layer neighboring the charged surfaces is essentially made of monovalent counterions extracted from the bulk electrolyte reservoir. At the experimental temperature of 28 °C with the relative permittivity of water of 77.22, the Debye's length of a monovalent electrolyte solution is $l_D = 0.304/\sqrt{c}$ nm with c in mol l^{-1}, giving an equivalent bulk concentration of monovalent electrolyte of 2.75 mM l^{-1} for $l_D = 5.8$ nm. With the monomer mass $M_A = 71.25$ g and the ionization ratio $f \simeq 0.25$, the solution of 0.8 g l^{-1} corresponds to a monovalent charge concentration of 2.77 mM l^{-1}, which is extremely close to the value deduced from the Debye's length. This supports the interpretation in terms of DLVO interaction and the electrostatic nature of the repulsive interaction force.

Thus, together with the stepped profile of the stiffness inside the contact, the picture emerging from the equilibrium interaction force is a solid/solution interface made of chains adsorbed in a thin layer, and creating a negative surface charge. The negatively charged surface is neighbored by an electrical double layer (EDL) made of positive monovalent ions. Polyelectrolyte adsorption on surface has been the focus of extensive studies, due in part to the technological importance of polyelectrolyte multilayers formed by the successive deposition of positively and negatively charged polyelectrolytes from aqueous solutions.[36] In the case of a low-salt concentration, which is the case here, the overcharge of the surface due to the chains adsorption is expected to be given by:[36]

$$\delta\sigma = e\frac{f^{1/3}}{u^{1/3} a l_D} \quad u = \frac{l_B}{a} \tag{11}$$

With the experimental value of the Debye's length $l_D = 5.8$ nm the above expression gives a surface charge of 35 mC m^{-2}. This theoretical value is very close to the experimental value issued from the DLVO fit of the repulsive force. A schematic picture of the interface structure is drawn in inset of Fig. 3.

4 Flow of semi-dilute solutions: thick films

Fig. 4 plots the components of the reduced mobility measured in a HPAM solution as a function of the sphere-plane distance. At distances larger than the micrometer, the variation of both components is essentially a straight line, as expected for a visco-elastic fluid. From eqn (8) the slope of these straight lines reflects the visco-elastic modulii of the solutions. Both components have the same order of magnitude, which demonstrates the strong visco-elastic character of the solutions. The plot also shows that the flow undergoes a partial slip boundary condition on the solid surfaces: the large distance variation of the dissipative part $\mu_R R^2$ is not linear but affine with the distance. It extrapolates to a finite ordinate at origin, pointing toward values of the solid–liquid coefficient in the range of 30 kPa s m^{-1}. To the contrary the conservative part $\mu_I R^2$ extrapolates toward origin within the experimental uncertainty, corresponding to a purely dissipative friction at the solid–liquid interface.

Precise values of the bulk modulii and Navier's partial slip boundary condition are determined by fitting the data to the full theory given by eqn (7) for the oscillating drainage flow of a visco-elastic liquid undergoing a Navier boundary condition. According to the experimental observation, we assume a purely dissipative friction coefficient $\tilde{\lambda} = \lambda_R$. The quantitative

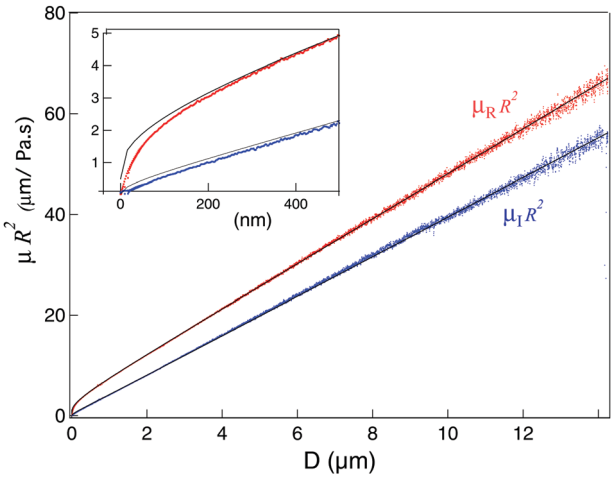

Fig. 4 Components of the reduced mobility $\tilde{\mu}R^2$ measured in an HPAM solution of 1 g l^{-1} at a frequency of 220 Hz. Red dots: dissipative part $\mu_R R^2$, blue dots: elastic part $\mu_I R^2$. The black lines are the components of expression (7) fitted with a real-valued Navier's friction coefficient $\tilde{\lambda} = \lambda_R$. Inset: Enlargement below the micrometric scale.

agreement with the data at distances larger than 200 nm is excellent (see inset of Fig. 4). It allows one to conclude that at large distance, the flow is indeed fully described by a slip boundary condition.

The measured values of the visco-elastic modulii of the HPAM solutions plotted in Fig. 5 depend on the concentration and on the driving frequency. The variation with the concentration is well described a power law in exponent 3/2 (dashed lines in Fig. 5). This is in good agreement with the theoretical expectations for polyelectrolyte solutions in the semi-dilute entangled regime,[36] which predict a scaling in $c^{3/2}$ for the steady-state shear viscosity and the plateau shear modulus. We observe that these scaling laws also hold for both components of the linear visco-elastic modulus measured here.

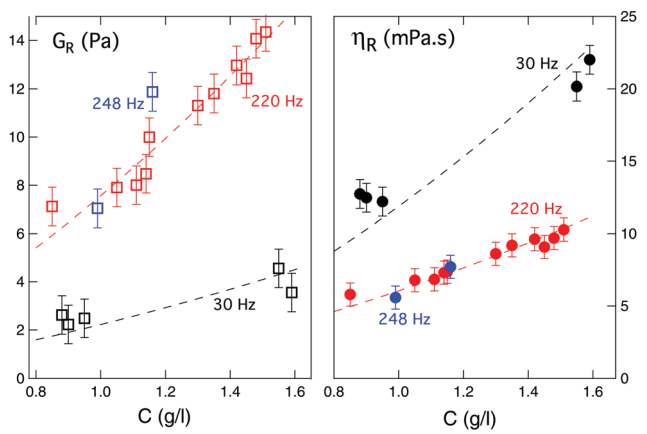

Fig. 5 Left graph: Shear modulus G_R at different frequencies (□) 30 Hz, (□) 220 Hz, (□) 248 Hz as a function of the HPAM concentration. The dashed lines are power-law fits in $c^{3/2}$, $G_R = Ac^{3/2}$. Right graph: Viscosity η_R as a function of the HPAM concentration (○) 30 Hz, (○) 220 Hz, (○) 248 Hz. The dashed lines are best power-law fits in $c^{3/2}$, $\eta_R = \eta_s + Bc^{3/2}$. The prefactors A and B depend on frequency.

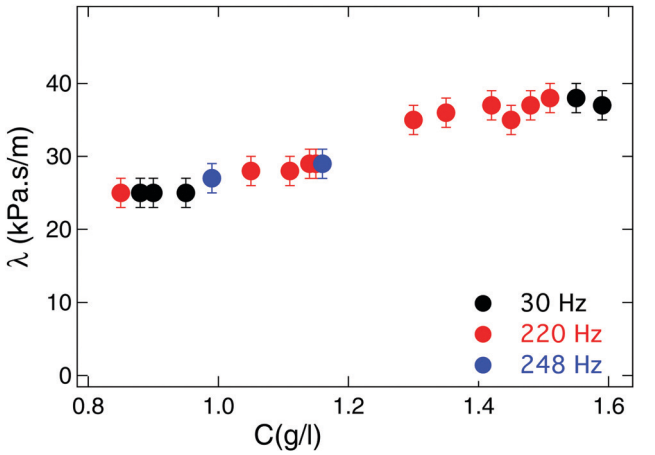

Fig. 6 Navier's friction coefficient of the HPAM solutions on the adsorbed layer, as a function of the concentration at different frequencies: 30 Hz (•), 220 Hz, (●) 248 Hz, (●) 248 Hz.

The values of the Navier's friction coefficient $\tilde{\lambda} = \lambda_R$ of the solutions are plotted in Fig. 6. The boundary friction is not only purely dissipative, but also independent of frequency in the range studied. This contrasts with the significant frequency dependency of the bulk modulii of the solutions. Thus, although the polyelectrolyte solutions are non-Newtonian complex fluids, their friction coefficient on the wall appears to be essentially Newtonian, real-valued and frequency independent.

In view of the equilibrium structure of the HPAM-solutions/solid interface depicted in Section 3, it is tempting to attribute the fully Newtonian Naviers' friction of the solutions on the solid walls to a depletion layer containing essentially pure solvent. Large wall slippage of polyelectrolyte solutions have indeed been reported previously in porous media, membranes,[17,45] surface force measurements,[29] as well as in solid-state nano-fluidic channels,[30] and attributed to a depletion layer at the solid/liquid interface. Assuming a depletion layer of pure water of viscosity 0.89 mPa s at the experiment temperature, the friction coefficients of Fig. 6 would correspond to values of the depletion layer thickness $e_d \approx \eta_{water}/\lambda_R \simeq 30$ nm, slightly decreasing when the concentration increases from 0.8 g l^{-1} to 1.6 g l^{-1}. These scales are fully resolved by our dynamic SFA; the next paragraph analyzes further the dynamic forces at this level of confinement.

5 Flow of semi-dilute solutions: thin films

The reduced mobility in a typical experiment (same as Fig. 4: HPAM concentration 1 g l^{-1}, 220 Hz) is plotted on Fig. 7 at small gap values, *i.e.*, sphere-plane distances below 30 nm. It is clear that the prediction of the partial slip boundary condition fitting the data at large scale, overestimates badly the dissipative component of the mobility. More specifically, we see that the dissipative component of the reduced mobility increases linearly with the sphere-plane gap, in a manner equivalent to

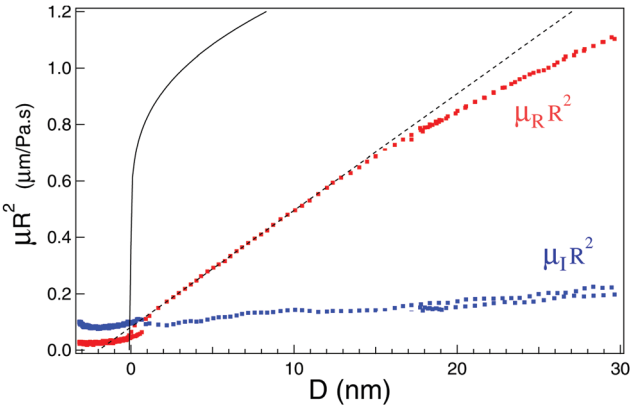

Fig. 7 Enlargement of Fig. 4 at small gap values: reduced mobility $\tilde{\mu}R^2$ of a HPAM solution of 1 g l^{-1} measured at 220 Hz. The black continuous line is the partial slip model plotted in Fig. 4, representing the best fit of the reduced mobility at large scale. The black dashed line is the reduced mobility of the sphere calculated for a Newtonian liquid of viscosity η_1 = 1.28 mPa s and a slip length of 1 nm on each side.

that of a liquid of viscosity η_1 flowing with a small slip length (1 nm) with respect to the chosen distance origin. The viscosity η_1 extracted from the slope is of 1.28 mPa s in this specific experiment, slightly larger than the viscosity of water at the experimental temperature (0.89 mPa s).

Thus, the dynamic measurements show directly the existence of a layer of reduced viscosity at the adsorbed polyelectrolyte/solution interface. A decrease of the effective viscosity of polyelectrolyte films with their thickness has already been observed in pioneering dynamic SFA experiments.[18,22] In hyaluronic acid confined between non-adsorbing mica surfaces, Tadmor *et al.*[22] found a linear decrease of the average viscosity below a gap of 400 nm, reaching the pure water viscosity at zero film thickness. Kuhl *et al.*[18] found a similar reduction of the average viscosity of aqueous polyethylene glycol films confined between bilayers. In both cases, the hydrodynamic force was interpreted in terms of effective liquid viscosity for a given value of the confinement, and the limit viscosity was found to be close to that of the solvent. Here the viscosity of the interfacial layer is slightly larger than the one of pure water. This could be due to an electro-viscous effect in the charged Debye's layer,[46] or, to the presence in this interfacial layer of polyelectrolyte chains with a very low concentration. We also note that the hydrodynamic origin, clearly resolved in these small gap dynamic measurements, lies about 2 nm beyond the arbitrarily chosen distance origin, which is the reception of the jump-to-contact of the surfaces. As the distance origin $D = 0$ corresponds to the contact between the top of the adsorbed layers, we see that a part of the adsorbed layers is indeed mobilised by the flow, over a thickness of 1 nm on each surface. The cumulated mobilised thickness (2 nm) is indeed very close to the total thickness of the layering forces observed in Fig. 3. Thus the adsorbed layers are able to resist to a significant normal force while keeping some mobility under a shear stress.

In order to determine more precisely the thickness of the depletion layer separating the adsorbed layer and the bulk semi-dilute solution, we develop a two-fluid flow model, incorporating on the top of the adsorbed layers, a depletion layer of thickness e and of viscosity $\tilde{\eta}_1$ meeting the bulk solution of visco-elasticity $\tilde{\eta}$ with a sharp viscosity contrast. The model assumes a lubrication flow in both fluids with a no-slip b.c. of the depletion layer onto the adsorbed layer. The latter is assumed not to participate in the flow. Finally we assume that the thickness e of the depletion layer is constant: this accounts for the fast diffusion of the solvent between the bulk and the depletion layer compared to the macroscopic time scale (given by the flow frequency or shear rate). No surface tension between the depletion layer and the bulk solution is taken into account. The reduced mobility writes (see Appendix):

$$\tilde{\mu}R^2 = \frac{D}{6\pi\tilde{\eta}}\left(f^*\left(\frac{D}{e}\right)\right)^{-1}$$

$$f^*(x \geq 2) = 2x\sum_{n=1}^{3}\alpha_n(x - A_n)\ln(1 - A_n/x)$$

$$f^*(x \leq 2) = 2x\sum_{n=1}^{3}\alpha_n(x - A_n)\ln\left(1 - \frac{A_n}{2}\right) + \frac{(x-2)^2}{4(\tilde{\delta}+1)} \quad (12)$$

$$\alpha_n = \frac{1}{12\tilde{\delta}(\tilde{\delta}+1)\gamma_n} \qquad A_n = -2\tilde{\delta}j^n\beta\gamma_n$$

$$\tilde{\delta} = \frac{\tilde{\eta}}{\tilde{\eta}_1} - 1 \qquad \gamma_n = \frac{1}{j^n\beta} + 1 + j^n\beta$$

$$(j^n\beta)^3 = \frac{1+\tilde{\delta}}{\tilde{\delta}} \qquad j = e^{2i\pi/3}$$

The factor f^* is calculated by taking for β anyone of the three complex cubic roots of the viscosity contrast $\tilde{\eta}/(\tilde{\eta} - \tilde{\eta}_1)$ as stated in the last equation of (12). Thus the three cubic roots of this contrast are $j\beta$, $j^2\beta$ and $j^3\beta = \beta$, and the sums involve a permutation over these three cubic roots.

At distance values $D \ll e$, the mobility reduces to $\tilde{\mu}R^2 \simeq D/6\pi\eta_1$ (see Appendix). Therefore the actual viscosity of the interfacial layers is determined directly from the slope of the components of $\tilde{\mu}R^2$ at small distance as in Fig. 7.

We compare the two-fluid model to the experimental data by keeping the value of the bulk visco-elastic modulus $\tilde{\eta}$ equal to that found in the thick film analysis. We also enforce a viscosity η_1 of the depletion layers coating the surfaces as measured from the data at small distances. Thus only the thickness e of the depletion layers is adjusted. Fig. 8 shows that in contrast to the partial slip model, the two-fluid model is in excellent agreement with the dissipative part of the mobility, from the macroscopic scale down to 3 nm, representing more than 3 orders of magnitude in gap size. This agreement is obtained for a unique value of the depleted layer thickness e. The two-fluid model is essentially identical to the partial slip boundary condition model at distances $D \geq 5e$. At smaller scale (stronger confinement) the finite thickness of the depletion layer at the wall interface cannot be ignored anymore, and the partial slip b.c. model becomes inaccurate, underestimating the viscous dissipation. The deviation with the data below 3 nm

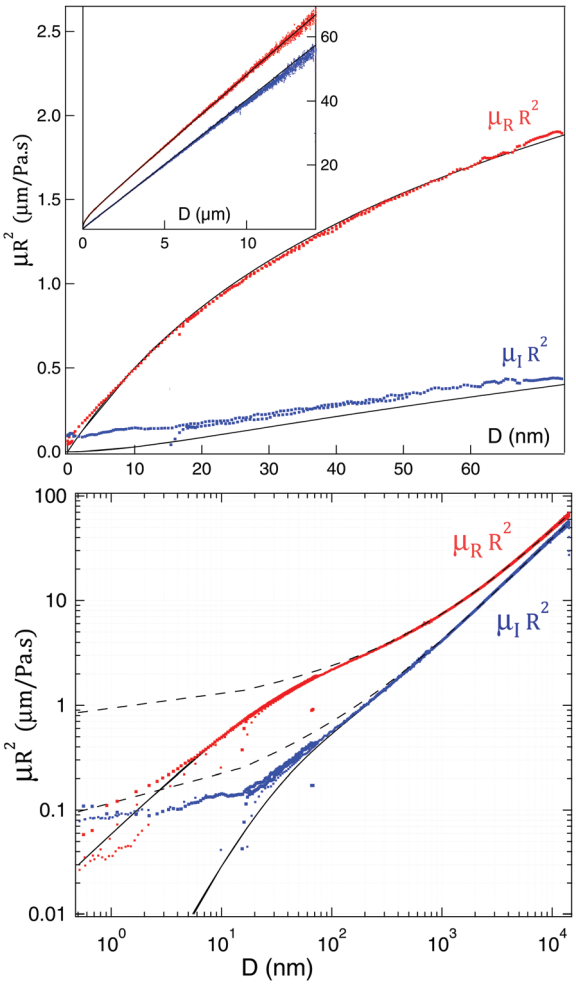

Fig. 8 Components of the reduced mobility in a HPAM solution of 1 g l^{-1} at 220 Hz (red: dissipative component, blue: elastic component) as a function of the sphere-plane distance. (a) Linear scale. The black continuous lines are the components of the two-fluid model (eqn (12)) calculated with e = 33 nm. The inset shows the plot at the micrometric scale. (b) log–log scale. The black dashed-line is the theory for a partial slip boundary condition enforced at D = 0 (eqn (6)).

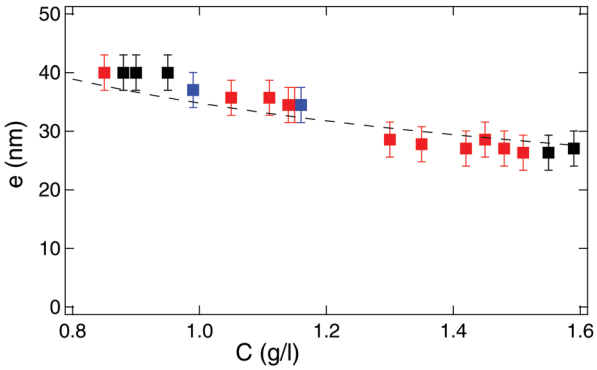

Fig. 9 Thickness e of the depletion layer obtained from the two-fluid model, as a function of the concentration of the solution C in g l^{-1}: (□) 30 Hz, (■) 220 Hz, (■) 248 Hz. The dashed black line plots the power-laws $y = (\xi + 2l_D)$ with ξ the correlation length of the semi-dilute solution and l_D the Debye's length.

is compatible with expected elasto-hydrodynamic effects due to the elastic deformation of the confining surfaces, as described in ref. 47 and 48.

Fig. 9 shows the thickness values e of the depleted layer obtained from the two-fluid model. The magnitude is in good overall agreement with the Navier's friction coefficient measured at large scale, $e \sim \lambda\eta_{water}$. In addition to be independent on the confinement, the depletion layer thickness is also independent on the flow frequency. Therefore the depletion layer is a fully equilibrium property of the solution/wall interface. It depends only on the solution concentration, ranging between 40 nm to 26 nm for HPAM concentrations varying from 0.8 to 1.6 g l^{-1}.

In view of the equilibrium structure of the solution/solid interface depicted in Section 3 we can compare the thickness of the depletion layer to two equilibria structural lengths: the correlation length ξ of the semi-dilute solution, and the Debye's length l_D screening the electrostatic interactions. Both ξ and l_D decay with the solution concentration in $c^{-1/2}$. The decay of the depletion layer by a ratio of 1.5 when the concentration increases by a factor of 2 is compatible with this scaling. More precisely the dashed line in Fig. 9 plots the quantity $\xi + 2l_D$, with $\xi = 23C^{-1/2}$ nm (see eqn (3)) and $l_D = 0.304\sqrt{M_A/fC} = 5.2C^{-1/2}$ nm. The depletion layer extracted from the 2-fluid model is rather well described by this phenomenological expression.

6 Discussion

Our experiments confirm the low friction of polyelectrolyte solutions on solid surfaces, as already observed in flow experiments involving other type of confined geometries (porous media, membranes,[17,45] solid-state nano-channels[30] and SFA[29]). Thanks to the concomitant characterisation of the equilibrium and dynamic features with our SFA, we can in addition establish three important properties of the polyelectrolyte solutions/solid surface.

The first important feature is that the apparent slip observed at large scale should be described with the original Navier's boundary condition, *i.e.* with an interfacial fluid friction coefficient, and not with a slip length.[40] This is required in order to separate the bulk rheological properties of the non-newtonian fluid from its interfacial rheology. We find a Newtonian interfacial friction coefficient not depending on frequency or shear-rate, and of value between 25 to 40 kPa s m^{-1} for our salt-free 20 M HPAM solutions of concentration between 0.8 to 1.6 g l^{-1}.

The second important property is that the apparent slippage of the solutions at the wall is due to an interfacial depletion layer at equilibrium, whose characteristics do not depend on the confinement, neither on the rate or frequency of the flow. This finding contrasts with the results of Cuenca *et al.*,[30] reporting a decrease in slip length and depletion layer of HPAM solutions, in nanochannels of decreasing height. However Cuenca *et al.* neglected the finite thickness of the depletion layer in their analysis of the effective viscosity under confinement. We show here, that if the channel height is comparable

or smaller than the apparent slip length measured at large scale, the apparent slip model severely underestimate the actual flow dissipation, leading to a spurious effect of confinement-dependant slippage and depletion layer.

The third important conclusion is the structure of the solution/solid interface and the origin of the depletion layers. We find that the polyelectrolyte chains adsorb on the solid surface in a thin nanometric adsorbed layer, as expected for solutions without added salt according to theoretical works.[42] The driving force for this adsorption is the image charge effect induced by the metallic substrates. This thin adsorbed layer confers a surface charge of more than 30 mC m^{-2} to the solid wall, in good quantitative agreement with theories describing the overcharging of surfaces due to polyelectrolyte adsorption. This surface charge is screened by the monovalent counterions, with a Debye's length coherent with their bulk concentration, and varying between 5.8 to 4.1 nm for our concentration range.

The charge of the adsorbed layer being of the same sign as the polyelectrolyte chains, it repells the chains of the solution, acting as an effective non-attracting solid surface. It is known from structural studies as well as from numerical models that the concentration of polymer solutions away from non-adsorbing boundaries is established over the correlation ξ characteristic of the bulk solution, leading to depletion layers of size ξ. More specifically, we find in our experiments that the thickness e of the depletion layers is in good quantitative agreement with a phenomenological expression $e = 2l_D + \xi$. Based on this phenomenological law we can propose the picture of the interface drawn in Fig. 10: the chains in solution behave as macro-ions of size ξ, screened by a Debye length l_D.

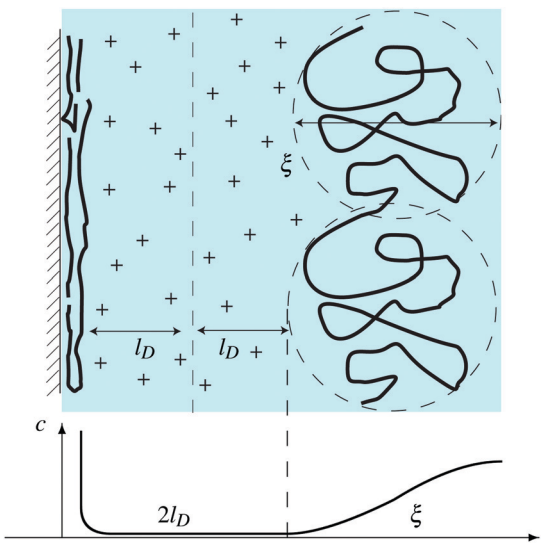

Fig. 10 Schematic of the interface: the polyelectrolyte chains in the solution behave as macro-ions of size ξ screened by the Debye's length l_D. They are repelled at a distance $2l_D$ from the charged adsorbed layer. The monomer concentration c is essentially zero over a distance $2l_D$ from the adsorbed layer, and increases gradually toward the bulk value over the correlation length ξ.

Due to the osmotic pressure of the cloud of counterions, the macro-ions are repelled from the adsorbed layer over a distance $2l_D$. Therefore the effective non-attracting wall for the chains in solution is located at a distance $2l_D$ from the top of the adsorbed layer. From this point the local viscosity should increase smoothly to reach the bulk value at $\xi + 2l_D$.

7 Conclusion

Thanks to a Dynamic Surface Force Apparatus we have measured in the same experiment the equilibrium interactions and hydrodynamic properties of confined polyelectrolyte solutions. This allows us to unravel the origin of the large slippage effect observed on the flow at a macroscopic scale, although the polyelectrolyte chains adsorb on the solid surface. We expect that these finding are of interest for communities studying the flow of solutions of charged macromolecules, such DNA or proteins. Work is presently in progress to investigate wider concentration range, polymer properties, and salinity of the solutions.

More generally this work paves the way for structural and dynamic investigation of complex liquids at the solid interface, which can be performed with the dynamic Surface Force Apparatus and with the Colloidal Probe AFM.

Conflicts of interest

There are no conflicts to declare.

Appendix: two-fluid model

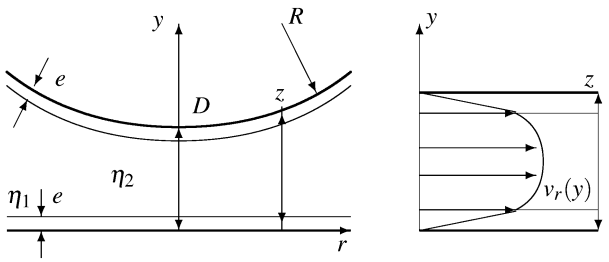

In this model the sphere and the plane are both covered with a liquid layer of thickness e and of viscosity η_1. The viscosity of the surrounding liquid is η_2, and $\delta = \eta_2/\eta_1 - 1$ is the relative excess viscosity. At small gap $D \ll R$, and if the sphere motion is slow compared to the diffusion time across the fluid films ($\dot{D} \ll \eta_1/\rho D$, with ρ the fluid density) the lubrication properties are met: the velocity profile $v_r(y)$ is parallel to the plane, the pressure $P(r)$ is uniform across the film thickness, and the average velocity is locally proportional to the pressure gradient:

$$u(r) = \frac{1}{z}\int_0^z v_r(y)\mathrm{d}r = -\frac{K(z)}{\eta_2}\frac{\mathrm{d}P}{\mathrm{d}r} \qquad (13)$$

The velocity profile obeys the Stokes equation in each phase, the no-slip b.c. on each solid surface, and the condition of

continuity of velocity and tangential stress at the two liquid interfaces. The velocity profile is:

$$\begin{aligned} 0 \le y \le e \quad v_r(y) &= \frac{\nabla P}{2\eta_1} y(y-z) e \le y \le \frac{z}{2} \\ v_r(y) &= \frac{\nabla P}{2\eta_2}\left(y^2 - z(y+\delta e) + \delta e^2\right) \frac{z}{2} \le y \le z \\ v_r(y) &= v_r(z-y) \end{aligned} \tag{14}$$

and the effective permeability $K(z)$ is:

$$\begin{aligned} z \ge 2e \quad K(z) &= K_2(z) \\ &= \frac{z^2}{12} + \frac{e}{2}\delta\left(z - 2e + \frac{4e^2}{3z}\right) \quad z \le 2e \\ K(z) &= K_1(z) = \frac{z^2\eta_2}{12\eta_1}. \end{aligned} \tag{15}$$

The volume conservation at velocity $\dot{D}$ writes:

$$2\pi r z u(r) = -\pi r^2 \dot{D} \tag{16}$$

Here we consider the total volume conservation only, and assume that the solvent exchange between the two phases ensures that the thickness e remains uniform.This leads, using (13) and the parabolic approximation $z = D + r^2/R$, to:

$$P(z) = -\frac{R\eta_2\dot{D}}{2}\int_z^\infty \frac{\mathrm{d}z'}{z'K(z')} \tag{17}$$

so that the hydrodynamic force writes:

$$F(D) = \int_0^\infty 2\pi r P(r) = -\pi R\eta_2\dot{D}\int_D^\infty \mathrm{d}z \int_z^\infty \frac{\mathrm{d}z'}{z'K(z')} \tag{18}$$

In an oscillatory flow at frequency $\omega/2\pi$ the forcing velocity is $\dot{D} = \mathrm{Re}[ih_0\omega \mathrm{e}^{i\omega t}]$. In the limit of linear response $h_0 \ll D$, all the dynamic quantities are harmonic functions of time at the forcing frequency, and are characterised by their complex amplitude only. In the above equations, only the terms in first order of h_0 are retained. The set of eqn (15) remains valid with the viscosities η_1, η_2 replaced by their complex visco-elastic analogous $\tilde{\eta}_1$ and $\tilde{\eta}_2$. Eqn (18) with η_2 replaced by the visco-elasticity $\tilde{\eta}_2$, gives the complex amplitude of the oscillating hydrodynamic force.

Defining the non-dimensional variable $\zeta = z/e$ and functions $\kappa_i(\zeta) = 12zK_i(z)/e^3$ (i = 1, 2) one get the following expressions:

$$\begin{aligned} F(D) &= -\frac{6\pi\eta_2 R^2\dot{D}}{D} f^*(D/e) \\ f^*(x) &= 2x\int_x^\infty \mathrm{d}\zeta \int_\zeta^\infty \frac{\mathrm{d}\zeta'}{\kappa(\zeta')} \\ \zeta \le 2 \quad \kappa(\zeta) &= \kappa_1(\zeta) = (\delta+1)\zeta^3 \\ \zeta \ge 2 \quad \kappa(\zeta) &= \kappa_2(\zeta) = \zeta^3 + 6\delta\zeta^2 - 12\delta\zeta + 8\delta \end{aligned} \tag{19}$$

The 3 complex roots of $\kappa_2(\zeta)$ are:

$$\begin{aligned} A_n &= -2\delta\left(1 + j^n\beta + j^{2n}\beta^2\right) \\ (j^n\beta)^3 &= \frac{1+\delta}{\delta} \quad j = \mathrm{e}^{2i\pi/3} \end{aligned} \tag{20}$$

(note that δ is a complex number) and its inverse decomposes in algebraic fractions as:

$$\begin{aligned} \frac{1}{\kappa_2(\zeta)} &= \sum_{n=1}^3 \frac{\alpha_n}{\zeta - A_n} \\ \alpha_n &= \frac{1}{12\delta(\delta+1)\gamma_n} \\ \text{with} \quad \gamma_n &= \frac{1}{j^n\beta} + 1 + j^n\beta \\ \text{and} \quad \sum_{n=1}^3 \alpha_n = 0 \quad \sum_{n=1}^3 \alpha_n A_n &= 0 \quad \sum_{n=1}^3 \alpha_n A_n^2 = 1 \end{aligned} \tag{21}$$

So that finally

$$f^*(x \ge 2) = 2x\sum_{n=1}^3 \alpha_n (x - A_n)\ln\left(1 - \frac{A_n}{x}\right) \tag{22}$$

$$f^*(x \le 2) = 2x\int_2^\infty \mathrm{d}\zeta \int_\zeta^\infty \frac{\mathrm{d}\zeta'}{\kappa_2(\zeta')} + 2x\int_x^2 \mathrm{d}\zeta\left\{\int_2^\infty \frac{\mathrm{d}\zeta}{\kappa_2(\zeta)} + \int_\zeta^2 \frac{\mathrm{d}\zeta'}{K_1(\zeta')}\right\} \tag{23}$$

$$f^*(x \le 2) = 2x\sum_{n=1}^3 \alpha_n (x - A_n)\ln\left(1 - \frac{A_n}{2}\right) + \frac{(x-2)^2}{4(\delta+1)} \tag{24}$$

Acknowledgements

This research was supported by the ANR program ANR-15-CE06-0005-02.

Notes and references

1 H. A. Barnes, *J. Non-Newtonian Fluid Mech.*, 1995, **56**, 221–251.
2 S. G. Hatzikiriakos, *Soft Matter*, 2015, **11**, 7851–7856.
3 A. Y. Malkin and S. Patlazhan, *Adv. Colloid Interface Sci.*, 2018, **257**, 42–57.
4 J. Israelachvili, *Intermolecular & Surface Forces*, Academic Press, London, 2nd edn, 1992.
5 N. Jaensson and J. Vermant, *Curr. Opin. Colloid Interface Sci.*, 2018, **37**, 136–150.
6 P. Auroy, L. Auvray and L. Leger, *Macromolecules*, 1991, **24**, 5158–5166.
7 C. Neto, D. R. Evans, E. Bonaccurso, H.-J. Butt and V. S. J. Craig, *Rep. Prog. Phys.*, 2005, **68**, 2859–2897.
8 J. D. McGraw, O. Bäumchen, M. Klos, S. Haefner, M. Lessel, S. Backes and K. Jacobs, *Adv. Colloid Interface Sci.*, 2014, **210**, 13–20.
9 M. Ebrahimi, V. K. Konaganti, S. Moradi, A. K. Doufas and S. G. Hatzikiriakos, *Soft Matter*, 2016, **12**, 9759–9768.

10 J. D. McGraw, T. S. Chan, S. Maurer, T. Salez, M. Benzaquen, E. Raphaël, M. Brinkmann and K. Jacobs, *Proc. Natl. Acad. Sci. U. S. A.*, 2016, **113**, 1168–1173.

11 M. Hénot, M. Grzelka, J. Zhang, S. Mariot, I. Antoniuk, E. Drockenmuller, L. Léger and F. Restagno, *Phys. Rev. Lett.*, 2018, **121**, 177802.

12 M. Ilton, T. Salez, P. D. Fowler, M. Rivetti, M. Aly, M. Benzaquen, J. D. McGraw, E. Raphaël, K. Dalnoki-Veress and O. Bäumchen, *Nat. Commun.*, 2018, **9**, 1172.

13 L. Fang and R. G. Larson, *Macromolecules*, 2007, **40**, 8784–8787.

14 L. Fang, H. Hu and R. G. Larson, *J. Rheol.*, 2005, **49**, 127–138.

15 Y. Cohen and A. B. Metzner, *J. Rheol.*, 1985, **29**, 67–102.

16 P. E. Boukany, O. Hemminger, S.-Q. Wang and L. J. Lee, *Phys. Rev. Lett.*, 2010, **105**, 027802.

17 G. Chauveteau, M. Tirrell and A. Omari, *J. Colloid Interface Sci.*, 1984, **100**, 41–54.

18 T. Kuhl, A. Berman, S. Hui and J. Israelachvili, *Macromolecules*, 1998, **31**, 8250–8257.

19 P. Cann and H. Spikes, *Tribol. Trans.*, 1994, **37**, 580–586.

20 M. A. Cohen Stuart, F. H. Waajen, T. Cosgrove, B. Vincent and T. L. Crowley, *Macromolecules*, 1984, **17**, 1825–1830.

21 E. Donath, A. Krabi, G. Allan and B. Vincent, *Langmuir*, 1996, **3425–3430**, 3425–3430.

22 R. Tadmor, N. Chen and J. Israelachvili, *J. Biomed. Mater. Res.*, 2002, **61**, 514–523.

23 Z. Li, L. D'eramo, F. Monti, A.-L. Vayssade, B. Chollet, B. Bresson, Y. Tran, M. Cloitre and P. Tabeling, *Isr. J. Chem.*, 2014, **54**, 1589–1601.

24 L. Auvray, P. Auroy and M. Cruz, *J. Phys.*, 1992, **2**, 1133–1140.

25 L. T. Lee, O. Guiselin, A. Lapp, B. Farnoux and J. Penfold, *Phys. Rev. Lett.*, 1991, **67**, 2838.

26 O. Vinogradova, *Langmuir*, 1995, **11**, 2213–2220.

27 J. Sanchez-Reyes and L. A. Archer, *Langmuir*, 2003, **19**, 3304–3312.

28 R. Horn, O. Vinogradova, M. Mackay and N. Phan-Thien, *J. Chem. Phys.*, 2000, **112**, 6424.

29 J. Cayer-Barrioz, D. Mazuyer, A. Tonck and E. Yamaguchi, *Tribol. Lett.*, 2008, **32**, 81–90.

30 A. Cuenca and H. Bodiguel, *Phys. Rev. Lett.*, 2013, **110**, 108304.

31 M. Graham, *Annu. Rev. Fluid Mech.*, 2011, **43**, 273–298.

32 J. A. Millan, W. Jiang, M. Laradji and Y. Wang, *J. Chem. Phys.*, 2007, **126**, 03B617.

33 R. Kekre, J. E. Butler and A. J. Ladd, *Phys. Rev. E: Stat., Nonlinear, Soft Matter Phys.*, 2010, **82**, 050803.

34 L. Lake, *Enhanced Oil Recovery*, Prentice-Hall, Inc., 1989.

35 D. Wever, F. Picchioni and A. Broekhuis, *Prog. Polym. Sci.*, 2011, **36**, 1558–1628.

36 A. Dobrynin and M. Rubinstein, *Prog. Polym. Sci.*, 2005, **30**, 1049–1118.

37 C. Malmberg and A. Maryott, *J. Res. Natl. Bur. Stand.*, 1956, **56**, 1–8.

38 L. Garcia, C. Barraud, C. Picard, J. Giraud, E. Charlaix and B. Cross, *Rev. Sci. Instrum.*, 2016, **87**, 113906.

39 B. Derjaguin, N. V. Churaev and V. Muller, *Surface Forces*, Plenum, New York, 1987.

40 B. Cross, C. Barraud, C. Picard, L. Léger, F. Restagno and E. Charlaix, *Phys. Rev. Fluids*, 2018, **3**, 062001(R).

41 P. Claesson, E. Poptosheva, E. Blomberg and A. Dedinaite, *Adv. Colloid Interface Sci.*, 2005, **114–115**, 173–187.

42 R. Netz and J.-F. Joanny, *Macromolecules*, 1999, **32**, 9013–9025.

43 B. Shklovskii, *Phys. Rev. Lett.*, 1999, **82**, 326871.

44 R. Tadmor, E. Hernandez-Zapata, N. Chen, P. Pincus and J. Israelachvili, *Macromolecules*, 2002, **35**, 2380–2388.

45 A. Omari, M. Moan and G. Chauveteau, *Rheol. Acta*, 1989, **28**, 520–526.

46 M.-C. Audry, A. Piednoir, P. Joseph and E. Charlaix, *Faraday Discuss.*, 2010, **146**, 113–124.

47 S. Leroy and E. Charlaix, *J. Fluid Mech.*, 2011, **674**, 389–407.

48 R. Villey, E. Martinot, C. Cottin-Bizonne, M. Phaner-Goutorbe, L. Leger, F. Restagno and E. Charlaix, *Phys. Rev. Lett.*, 2013, **111**, 215701.